JCI insight

RESEARCH ARTICLE

Chimeric antigen receptor costimulation domains modulate human regulatory T cell function

Angela C. Boroughs,[1,2] Rebecca C. Larson,[1,2] Bryan D. Choi,[1,3] Amanda A. Bouffard,[1] Lauren S. Riley,[1] Erik Schiferle,[4] Anupriya S. Kulkarni,[5] Curtis L. Cetrulo,[6] David Ting,[5,7,8] Bruce R. Blazar,[9] Shadmehr Demehri,[4,5,8] and Marcela V. Maus[1,5,7,8]

[1]Cellular Immunotherapy Program, Massachusetts General Hospital, Boston, Massachusetts, USA. [2]Harvard Immunology Program, Harvard Medical School, Boston, Massachusetts, USA. [3]Department of Neurosurgery and [4]Department of Dermatology, Massachusetts General Hospital, Boston, Massachusetts, USA. [5]Massachusetts General Hospital Cancer Center, Boston, Massachusetts, USA. [6]Division of Plastic Surgery and [7]Division of Hematology and Oncology, Department of Medicine, Massachusetts General Hospital, Boston, Massachusetts, USA. [8]Harvard Medical School, Boston, Massachusetts, USA. [9]Department of Pediatrics, University of Minnesota, Minneapolis, Minnesota, USA.

Tregs are key modulators of inflammation and are important for the maintenance of peripheral tolerance. Adoptive immunotherapy with polyclonal Tregs holds promise in organ transplantation, graft-versus-host disease, and autoimmune diseases but may be enhanced by antigen-specific, long-lived Tregs. We modified primary human Tregs with chimeric antigen receptors (CARs) bearing different costimulatory domains and performed in vitro analyses of their phenotype and function. While neither the presence of a CAR nor the type of costimulation domain influenced Foxp3 expression in Tregs, the costimulation domain of the CARs affected CAR-Treg surface phenotype and functions, such as cytokine production. Furthermore, signaling from the CD28 costimulation domain maintained CAR-Treg suppressor function, whereas 4-1B costimulation did not. In vivo, CAR-Tregs accumulated at sites expressing target antigen and suppressed antigen-specific effector T cell responses; however, only CAR-Tregs with CD28 signaling domains were potent inhibitors of effector T cell–mediated graft rejection in vivo. Our findings support the use of CD28-based CAR-Tregs for tissue-specific immune suppression in the clinic.

Introduction

Tregs are lymphocytes that function to suppress excessive immune responses, regulate tolerance to self-antigens, and maintain tissue integrity (1). Adoptive transfer of Tregs in preclinical mouse models and human trials has demonstrated therapeutic potential in solid organ transplantation (2, 3), graft-versus-host disease (GvHD) (4–8), and a range of autoimmune diseases (9–13). Analogous to T cell therapy for cancer, where adoptive transfer of polyclonal ex vivo–stimulated conventional T cells (Tconvs) had modest antitumor effects (14), we and others have hypothesized that antigen-specific Tregs with enhanced persistence could augment the efficacy of Treg therapy (15–18).

Genetic redirection of Tconvs with chimeric antigen receptors (CARs) has enabled polyclonal peripheral blood T cells to be redirected to a specific tumor-associated antigen (19, 20). First-generation CARs contained only an extracellular antigen-binding domain, a transmembrane domain, and the signaling domain of CD3ζ, all fused in tandem as one molecule (21, 22). These CAR T cells did not mediate significant antitumor activity or persist in patients. Second-generation CARs included intracellular costimulatory domains, derived from either CD28 or 4-1BB. Second-generation CD19-directed CAR T cells had enhanced proliferation, persistence, and antitumor activity in both mouse models (23, 24) and early-phase clinical trials (25, 26), ultimately leading to their approval as therapeutics for patients with B cell malignancies (27). Although both CD28- and 4-1BB–based CARs have remarkable efficacy, the CD28 and 4-1BB costimulation domains in Tconvs result in different in kinetics, persistence, and toxicity profiles in patients (28, 29). Only CARs containing the 4-1BB costimulatory domain have demonstrated persistence beyond 6 months (30) and, in some cases, over 8 years (28).

Conflict of interest: ACB and MVM are listed as inventors on patents (US Provisional Application 62/573,242) filed that are relevant to this work; patents are held by Massachusetts General Hospital and have not been licensed as of this submission.

Submitted: November 14, 2018
Accepted: March 11, 2019
Published: April 18, 2019.

Reference information: *JCI Insight*. 2019;4(8):e126194. https://doi.org/10.1172/jci.insight.126194.

To date, there has been no systematic investigation of which costimulation domain best maintains the phenotype and function of CAR-Tregs while increasing their proliferation, survival, and persistence. Others have used CD28-based CARs in Tregs and have demonstrated antigen-specific immunosuppressive activity with CAR-Tregs directed to factor VIII and HLA-A2 in preclinical xenogeneic models of anti-VIII responses to factor VIII replacement for hemophilia and GvHD, respectively (31–33). Although CD28 costimulation is known to be important for Treg activation and function (34, 35), in a preclinical model, CD28-based CAR-Tregs (anti–HLA-A2-28ζ) persisted for fewer than 3 weeks in NSG mice (31). Data on the role of 4-1BB activation in Tregs are less clear, with one report that 4-1BB activation can improve Treg expansion (36), while another found that 4-1BB signaling inhibits Treg suppression (37).

We therefore sought to investigate the effects of CD28 and 4-1BB second-generation CARs in Tregs, with the hypothesis that CARs bearing different intracellular domains would result in differential Treg phenotypic stability, persistence, and immunosuppressive function.

Results

Isolation of Tregs and transduction with CARs bearing different signaling domains. Tregs from healthy donor leukopacks were first enriched for $CD25^+$ cells by magnetic selection and then purified by FACS sorting based on expression of the surface markers $CD4^+$ and $CD25^{++}CD127^{lo}$ (Figure 1A). In parallel, we sorted $CD4^+CD25^{lo}$ Tconvs as controls from the same donor in each experiment (Figure 1A). Sorted human Tregs were confirmed to express intracellular Foxp3 (Figure 1B and Supplemental Figure 1A; supplemental material available online with this article; https://doi.org/10.1172/jci.insight.126194DS1) and were demethylated at the Treg-specific demethylation region (TSDR) of the X chromosome (Figure 1C). Sorted Tregs also expressed higher levels of phenotypic markers that differentiate resting Tregs from Tconvs, including CD39 and the latency-associated peptide (LAP) (Supplemental Figure 1B). Surface expression of CTLA4 and LAG3 was undetectable, as expected for nonactivated Tregs (Supplemental Figure 1B).

We synthesized 4 different anti-CD19 CAR constructs in a lentiviral vector backbone (Figure 1D): a control CAR construct that contained a truncated, nonsignaling CD3ζ chain (Δζ); a first-generation CAR (ζ); and 2 second-generation CARs, one with a CD28 (28ζ) and the other with a 4-1BB (BBζ) costimulation domain. All CARs had the same single-chain variable fragment (scFv) against CD19 with identical CD8 hinge and transmembrane domains. An mCherry fluorescent reporter gene was included downstream of the CAR construct after a T2A element to facilitate evaluation of CAR transduction. Immediately after sorting, Tregs and Tconvs were activated and then transduced with the lentiviral vectors. CAR-Tregs were then expanded for 1 week and rested for 1 week in media containing rhIL-2. In this time, Tregs expanded by 5 population doublings (32-fold) (Supplemental Table 1). At 2 weeks from initial isolation, CAR-Tregs were phenotyped and used in functional assays (Figure 1E). Although we did not observe any differences in transduction efficiencies among the different CARs in Tregs (1-way ANOVA, $P = 0.455$), we did find that the transgenes were expressed at higher levels in Tregs compared with Tconvs, despite using the same multiplicity of infection (MOI), as has been described (ref. 31 and Figure 1F).

CAR-Tregs retain Foxp3 expression in culture irrespective of their CAR signaling domains. CAR-modified Tregs were analyzed for the expression of Foxp3 and the methylation status of the TSDR, CTLA-4 promoter, and Helios promoter, an additional transcription factor important for maintenance of the Treg lineage (38). We analyzed resting time points after manufacturing (day 14, when CAR-Tregs would be harvested/infused) or after antigen stimulation (day 23) through either their TCR or CAR. Resting time points were chosen because many Treg-associated markers, including both CD25 and Foxp3, are expressed in Tconvs during activation (39). Antigen stimulation was performed by coculture of CAR-Tregs with irradiated K562-based artificial antigen-presenting cells (APCs) transduced to express either membrane-bound anti-CD3 or native CD19. Intracellular Foxp3 staining demonstrated that at harvest (day 14) and following antigen stimulation through the CAR or TCR, CAR-Tregs remained $Foxp3^+$ irrespective of the CAR construct (Figure 2A and Supplemental Figure 1C). Demethylation of the TSDR locus also remained stable after isolation (day 0), through harvest (day 14), and following antigen stimulation through the CAR (day 23) (Figure 2B). Untransduced Tregs behaved identically to Δζ CAR-Tregs. For example, TSDR methylation status was unchanged by the expression of the Δζ CAR (Supplemental Figure 1D), but for clarity, we chose to display only Δζ CAR-Tregs in the remaining figures. The mean methylation of *CTLA4* (Figure 2C) and *IKZF2* (Helios, Supplemental Figure 1E) loci was lower in all CAR-Tregs compared with CAR-Tconvs at day 0 and remained stable through transduction/harvest (day 14) and restimulation (day 23), independent of the CAR construct.

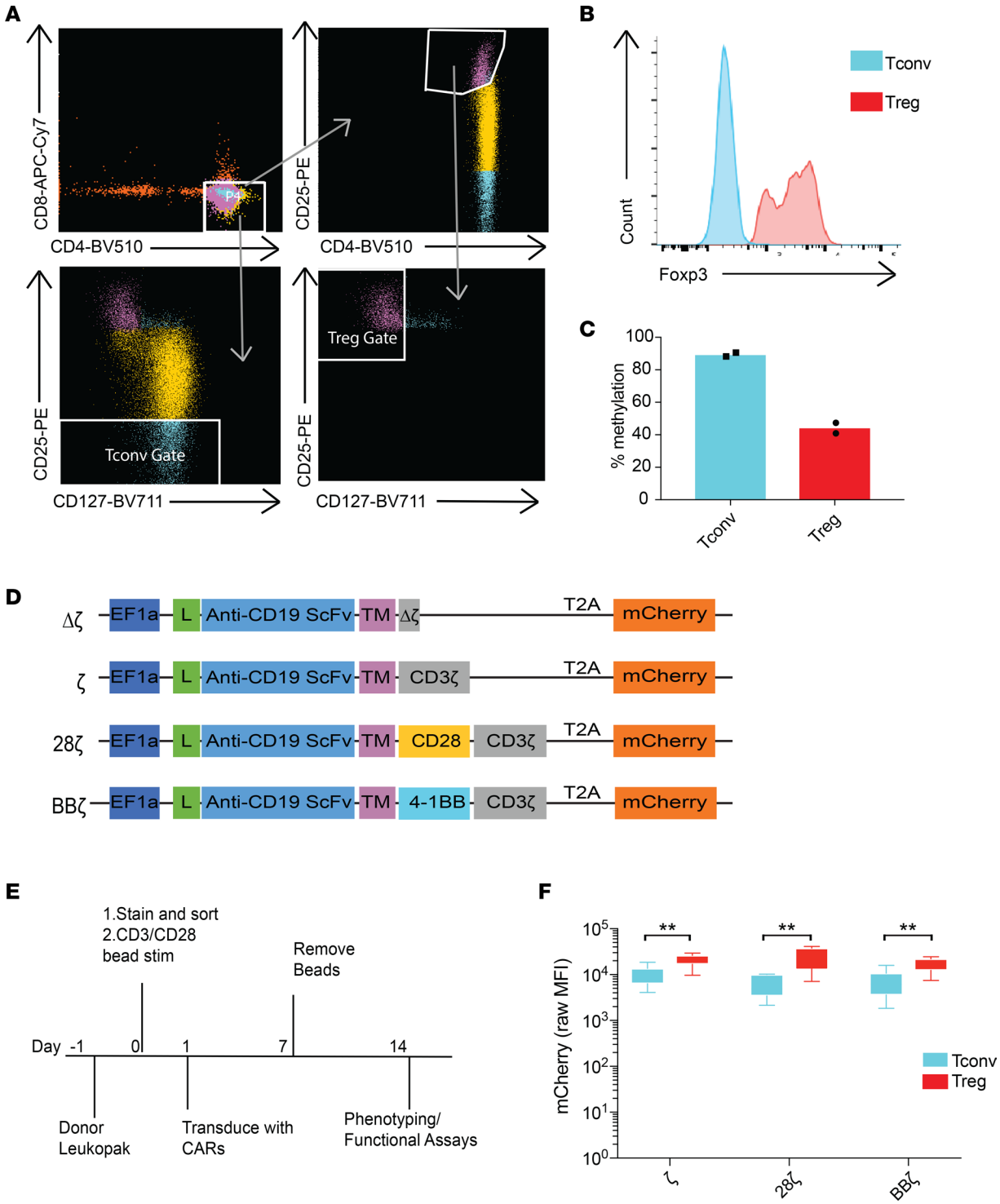

Figure 1. Generation of CAR-Tregs. CD4⁺ T cells were isolated from human donor peripheral blood mononuclear cells (PBMCs) and enriched for CD25⁺ cells using positive selection. (**A**) Sorting gates for Tregs: $CD4^{mid}$, $CD25^{++}$, and $CD127^{lo}$. Sorting gates for Tconvs: $CD4^{+}$ and $CD25^{lo}$. Gates were drawn on cells prior to CD25 enrichment. (**B**) Foxp3 (clone PCH101) intracellular stain after sort. Data are representative of 7 independent sorts from different human donors. (**C**) Methylation status averaged across sites in the Treg-specific demethylation region (TSDR) on the X chromosome of the sorted T cell populations from female-donor leukopacks (n = 2 female donors, mean plotted). Dots within bars represent individual data points. (**D**) Vector maps of CD19 CAR constructs. L, leader sequence; scFv, single-chain variable fragment; TM, hinge and transmembrane domain. (**E**) Experimental design and preparation of CAR-Tregs. (**F**) Whiskers plots showing mCherry mean fluorescence intensity (MFI) of CAR T cells 12 days after lentivirus transduction at an MOI of 5 measured by flow cytometry (n = 7 human donors). **adj-P < 0.01, by paired ratio t test with Holm-Bonferroni method adjustment for 3 tests between Tregs and Tconvs. Tr, Treg; Tc, Tconv.

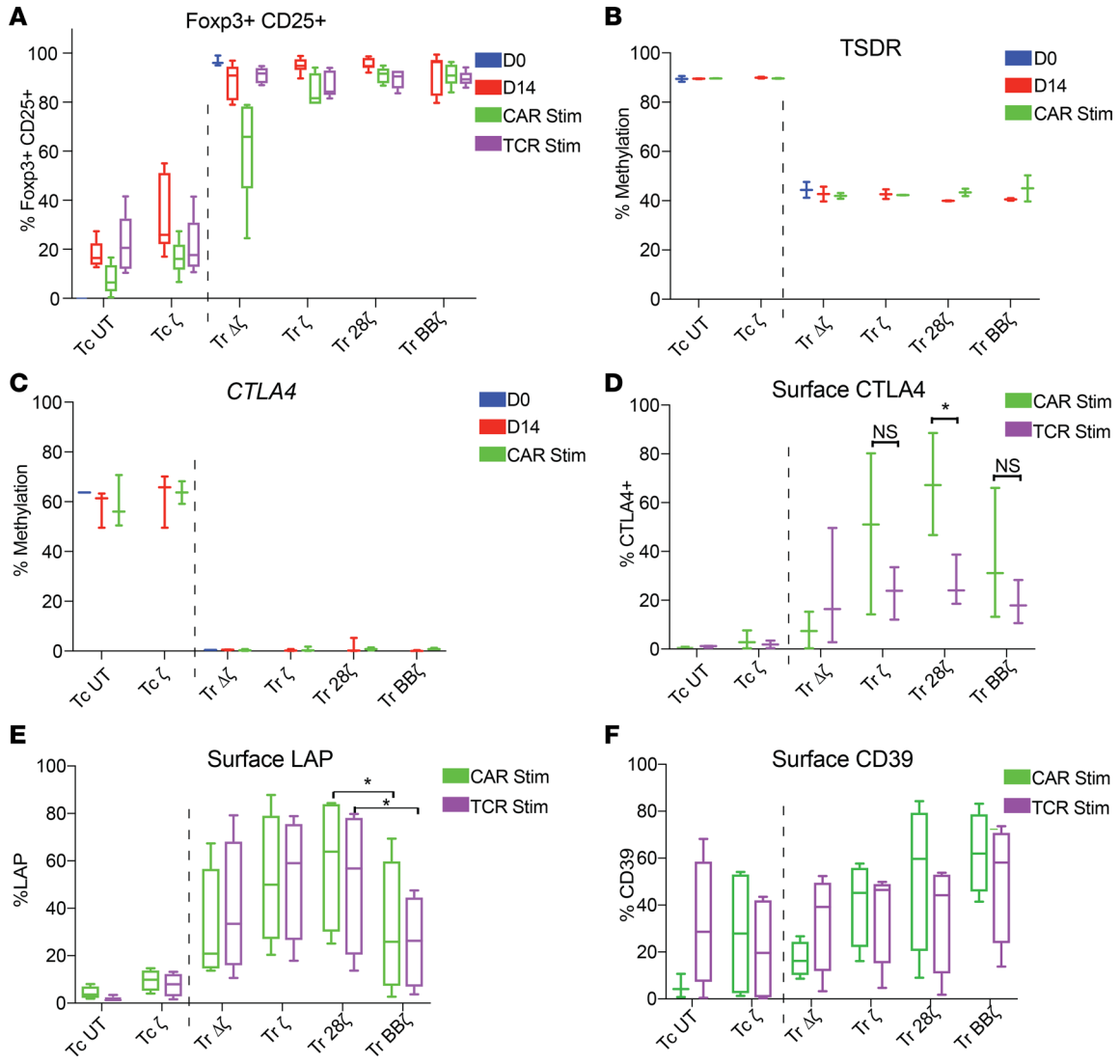

Figure 2. Foxp3 expression is stable after transduction, bead expansion, and restimulation. (**A**) Intracellular staining of Foxp3 and CD25 as a percentage of total $CD3^+CD4^+mCherry^+$ after sorting (day 0), bead expansion, and rest (day 14) and on day 23, 9 days after the addition of irradiated anti-CD3 K562 (TCR stim) or CD19-K562 (CAR stim) (n = 6 human donors). Methylation status using direct bisulfite modification and pyrosequencing of (**B**) the TSDR (n = 2 human female donors) and (**C**) the *CTLA4* promotor (n = 3 human donors) on day 0 after sort, day 14, and day 23 with CAR stimulation. Surface expression of (**D**) CTLA4, (**E**) LAP, and (**F**) CD39, 9 days after TCR or CAR stimulation with irradiated K562 cells ($n \geq 3$ human donors). All data are represented as box-and-whisker plots. *Adj-$P < 0.05$ by paired t test for CAR stimulation versus TCR stimulation (**D**) and between Tr 28ζ and Tr BBζ (**E**) with Holm-Bonferroni method adjustment for 3 and 2 tests, respectively. Blue bars for D0 represent UT Tregs and UT Tconvs immediately after sort. Tc, Tconvs; Tr, Treg.

We next analyzed CAR-Tregs for surface expression of the classic Treg functional markers CTLA4, LAP, and CD39 after stimulation through their CAR or TCR. Overall, antigen stimulation of Tregs resulted in a higher frequency of CTLA surface expression than in Tconvs (Figure 2D). Furthermore, antigen stimulation through CD28-based CARs induced significantly more CTLA4 expression than stimulation though the TCR in CAR-Tregs (Figure 2D), as has been reported (31). There were no statistically significant differences in surface CTLA4 expression when ζ, 28ζ, or BBζ CARs were engaged and compared with each other, and there was no difference when comparing ζ or BBζ stimulation to stimulation through the TCRs in the same cells (Figure 2D). We also wanted to investigate whether the costimulation domain affected surface LAP expression. To this end, we found that 28ζ CAR-Tregs had higher LAP expression than BBζ CAR-Tregs when stimulated through their CAR or TCR (Figure 2E), indicating that the mere presence of the CAR altered the activation-induced expression of LAP. CD39 expression did not significantly differ across different kinds of CAR-Tregs (Figure 2F) or after stimulation through the CAR or TCR. From these results, we conclude that the expression of a CAR and the type of costimulation domain

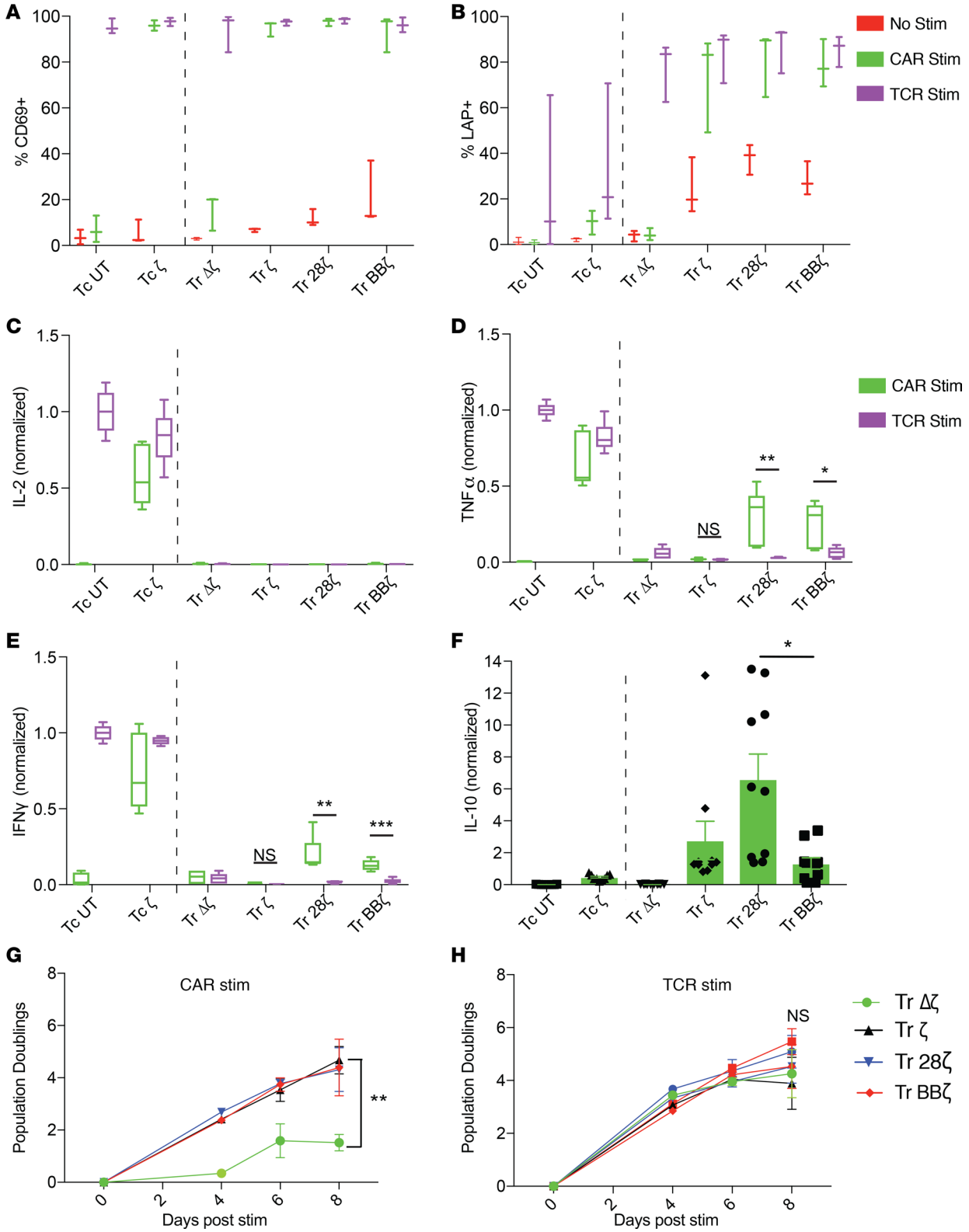

Figure 3. CAR-Tregs can be activated through their CAR or their TCR. T cells were left unstimulated or stimulated with irradiated CD19-K562 (CAR stim) or anti-CD3-K562 (TCR stim) at a 1:1 ratio for 20 hours on day 14 followed by surface staining of (**A**) CD69 and (**B**) latent-associated peptide (LAP), measured as a percentage, after gating live mCherry$^+$CD4$^+$ T cells, except in the case of the UT groups, which were only gated on live CD4$^+$ T cells (n = 3 human donors). Supernatants were saved 20 hours after T cell/K562 coculture to measure (**C**) IL-2, (**D**) TNF-α, and (**E**) IFN-γ in parallel. Cytokine levels were normalized to Tconv UT stimulated with K562-OKT3 (baseline quantification, IL-2, 7.03 ng/ml; TNF-α, 1.69 ng/ml; IFN-γ, 2.58 ng/ml; n = 3 human donors). (**F**) IL-10 detected in the supernatants of T cell and CD19-K562 cocultures (n = 5 human donors, baseline quantification of Tc UT stimulated with K562-OKT3 was 380 pg/ml). No cytokines were detected in the wells with K562 cells alone or with T cells alone. Live T cell number counted over time,

expressed as the $\log_2$ fold change of the starting cell number before K562 stimulation (day 14) after (**G**) CD19 or (**H**) anti-CD3 stimulation (n = 3 human donors). *adj-P < 0.05, **adj-P < 0.01, ***adj-P < 0.001, by paired t test with Holm-Bonferroni method adjustment for 3 tests (**D** and **E**). Significance was determined between functional CAR T cells in **F** by 1-way ANOVA with Tukey's multiple comparisons test. *P < 0.05, by paired t test for **G** and **H**, with significance calculated at day 8 between Tr Δζ and Tr 28ζ. Data represents box-and-whisker plots (**A**–**E**) or mean ± SEM (**F** and **G**). Tc, Tconvs; Tr, Treg. Dots within bars represent individual data points (**F**).

do not affect Foxp3 stability or the methylation status of *CTLA4* and *IKZF2* promotors. However, transduction with CARs and signaling through the CAR can effect the expression of Treg phenotypic surface markers CTLA4 and LAP, with 28ζ CAR increasing the expression of both markers.

CAR-Tregs stimulated through either their CAR or endogenous TCR upregulate Treg activation markers, produce cytokines, and proliferate. Tregs need to be activated to become suppressive (40, 41). We measured the expression of activation markers in CAR-Tregs after 24 hours of in vitro stimulation with APCs to engage their CAR or TCR. Like CAR-Tconvs, all functional (i.e., not Δζ) CAR-Tregs upregulated CD69 in response to both CAR and TCR activation (Figure 3A). In contrast, only Tregs and not Tconvs expressed high amounts of LAP after CAR or TCR activation (Figure 3B). Interestingly, functional CAR-Tregs expressed higher amounts of LAP at rest compared with ζ Tregs, suggesting tonic signaling from the CAR that results in expression of a Treg-specific surface protein. 4-1BB is also an activation marker in Tconvs and Tregs (42) and was upregulated after stimulation through CARs or TCRs in both Tconvs and Tregs. Interestingly, BBζ CAR-Tregs expressed higher levels of surface 4-1BB at baseline compared with all other CARs, but this difference disappeared after stimulation (Supplemental Figure 1F).

We analyzed the cytokine profiles in the supernatants of CAR-Tregs activated for 24 hours with artificial APCs. CAR-Tconvs produced high amounts of inflammatory cytokines (IL-2, TNF-α, IFN-γ) relative to CAR-Tregs (Figure 3, C–E). Cytokines were not detected in resting Tconv or Treg supernatants (data not shown). We noted, however, that CAR stimulation in 28ζ and BBζ CAR-Tregs induced low but significant levels of TNF and IFN-γ and compared with ζ CAR-Tregs or CAR-Tregs activated through their TCR. In contrast, we also found that CAR-Tregs produced higher amounts of IL-10 in response to CAR stimulation than Tconvs and that 28ζ CAR-Tregs produced significantly more IL-10 than BBζ Tregs (Figure 3F). CAR-Tregs also proliferated in response to either CAR (Figure 3G) or TCR stimulation (Figure 3H), except in the case of Δζ CAR-Tregs, which as expected, did not proliferate in response to CAR stimulation. Altogether, we conclude that ζ, 28ζ, and BBζ CAR-modified Tregs can be activated to proliferate through their CAR while maintaining their Treg identity based on surface phenotype and cytokine profile.

4-1BB costimulation specifically reduces CAR-mediated Treg suppressive function. Next, we tested CAR-Treg suppressive function toward T effector cells (Teffs). (Note that to avoid confusion, T cells — either $CD4^+$ alone or bulk $CD4^+$ and $CD8^+$ as specified for each experiment — suppressed by Tregs either in vitro or in vivo are referred to as Teffs, while T cells sorted as $CD4^+CD25^{lo}$ with the purpose of being directly compared with Tregs are referred to as $CD4^+$ Tconvs). To measure CAR-mediated Treg suppression in an antigen-specific manner, we needed a system whereby Teffs could be activated without anti-CD3 stimulation (which would result in stimulation of CD3 in the untransduced Tregs). Although we would have preferred to suppress a more "natural," TCR-mediated Teff response, when we used Raji cells to induce an allogeneic Teff response, we found that the Raji cells also activated allogeneic-untransduced Tregs, thus making the interpretation of CAR antigen–specific suppression impossible to distinguish or measure. Instead, we chose to use $CD4^+$ Teffs transduced to express the CD19-ζ CAR as the cells to be suppressed and irradiated $CD19^+$ Nalm6 cells as the target antigen-expressing cells in mixed lymphocyte reactions (MLRs). We specifically chose a first-generation CAR-Teff because CD19-ζ CAR-Teffs were more amenable to suppression than 28ζ (Supplemental Figure 2A) or BBζ (Supplemental Figure 2B) CAR-Teffs. Although ζ and 28ζ CAR-Tregs could inhibit proliferation of $CD4^+$ Teffs, BBζ CAR-Tregs could only minimally suppress proliferation, while Δζ CAR-Tregs did not suppress proliferation (Figure 4A); this result indicated that CAR signaling, but not antigen competition, is required to induce suppression. In experiments with bulk $CD4^+CD8^+$ CAR-Teffs, gating on the $CD8^+$ Teffs demonstrated that BBζ CAR-Tregs were also less efficient at suppressing $CD8^+$ Teff proliferation (Supplemental Figure 2C). We next measured inflammatory cytokines in supernatants of the MLRs, expecting that CAR-Tregs would inhibit the secretion of these cytokines by CAR-Teffs. For these experiments, we used $CD4^+$CD19-28ζ CAR-Teffs because they secrete the greatest amounts of cytokines, enhancing the dynamic range of our assay. Again, we found that BBζ CAR-Tregs were not as effective as 28ζ or ζ CAR-Tregs at lowering the secretion of TNF-α, GM-CSF, IL-2, and IFN-γ from Teffs (Figure 4, B–E, respectively).

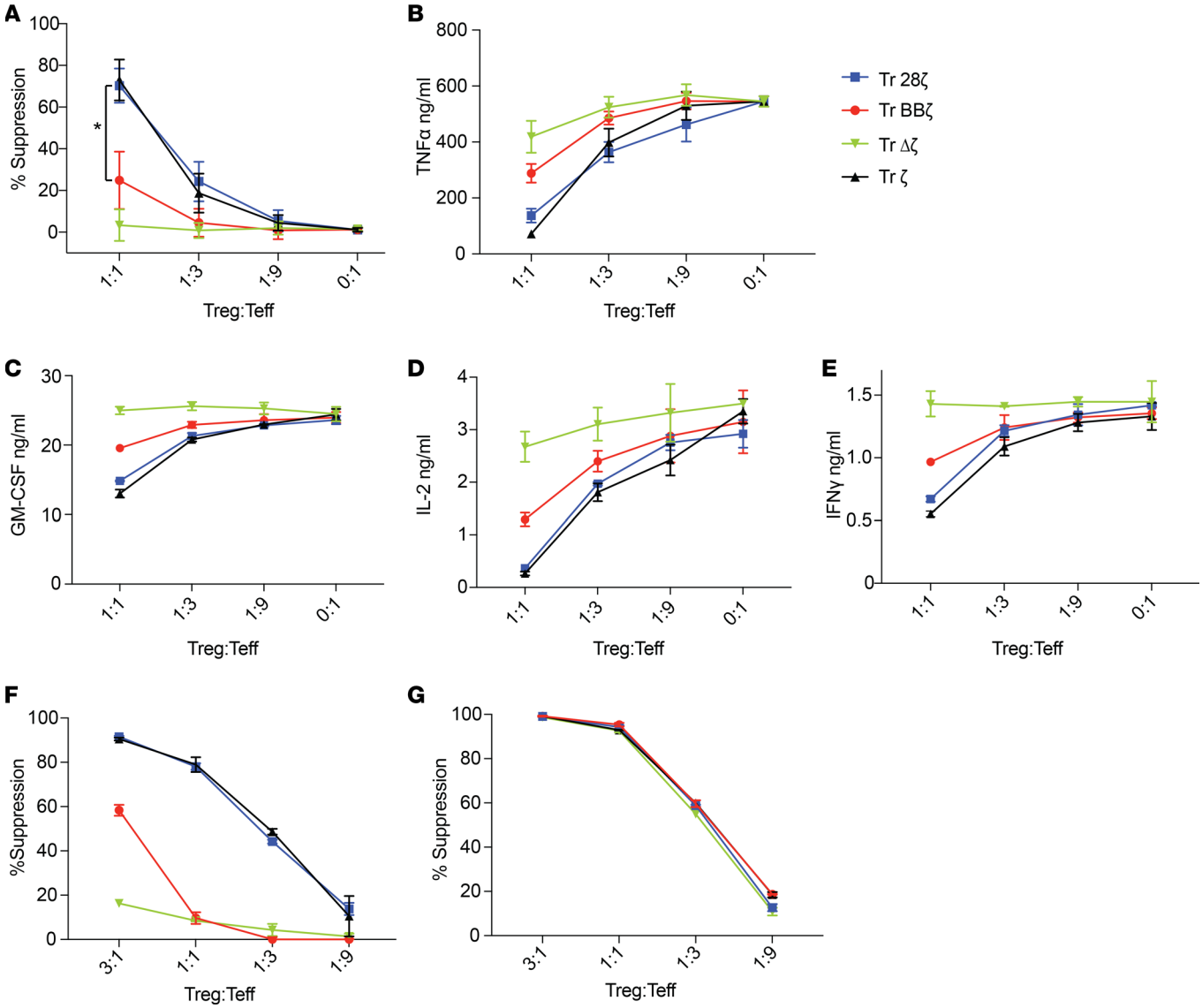

Figure 4. 4-1BB costimulation decreases CAR-Treg suppressive function. (**A**) MLRs of CFSE-labeled CD19 ζ CAR-Teffs cultured with indicated ratios of violet-labeled CD19 CAR-Tregs. After 3 days, CFSE dilution of the mCherry$^+$ Teff population was measured by flow cytometry to calculate suppression as a percentage of [1 – (number of CFSE^{lo} cells in the Treg condition)/(the number of mCherry$^+$ Teffs proliferating with no Tregs present]; (n = 5 human donors)]. Data represent mean ± SEM. *$P < 0.05$, paired t test performed for 1:1 Treg-to-Teff ratio comparing only BBζ and 28ζ. Supernatants were also collected in the same MLR, except with 28ζ CAR-Teffs as the CFSE-labeled cells. After 24 hours, cytokine levels of (**B**) TNF-α, (**C**) GM-CSF, (**D**) IL-2, and (**E**) IFN-γ were measured. MLRs comparing Treg suppression of Teff proliferation after activation though (**F**) the CAR (CFSE-labeled CD19 ζ CAR-Teffs, irradiated Nalm6 targets, 1:2 Teff-to-target cell ratio) or (**G**) the TCR (CFSE-labeled naive T cells, anti-CD3/anti-CD28 beads, 10:1 cell-to-bead ratio). After 4 days, CFSE dilution was measured). (**B**–**G**) Data are representative of 3 human donors, with technical triplicates. Mean and SEM of the triplicates plotted. Tr, Tregs.

Overexpression of CARs in T cells has been shown to result in ligand-independent constitutive signaling (43). To determine whether the decrease in suppressive capacity seen in the BBζ CAR-Tregs was caused by specific triggering of the BBζ CAR versus constitutive signaling through it, we repeated the MLR experiments but using either CD19$^+$ targets or anti-CD3/anti-CD28 beads for pan–T cell activation in parallel. We found that, in contrast, to the reduced suppression observed by triggering the BBζ CAR (Figure 4F), all CAR-Tregs stimulated through their TCR could equally suppress Teffs (Figure 4G). We conclude that the 4-1BB costimulation domain included in the CAR only inhibits Treg suppressive function when the CAR is engaged, rather than permanently altering the suppressive functions of TCR signaling in Tregs.

We sought to explore the mechanism of reduced immunosuppression in BBζ CAR-Tregs but were unable to conclusively pinpoint a dominant factor. Tregs are thought to suppress Teff proliferation through a variety of mechanisms, including the secretion of inhibitory cytokines TGF-β and IL-10 and

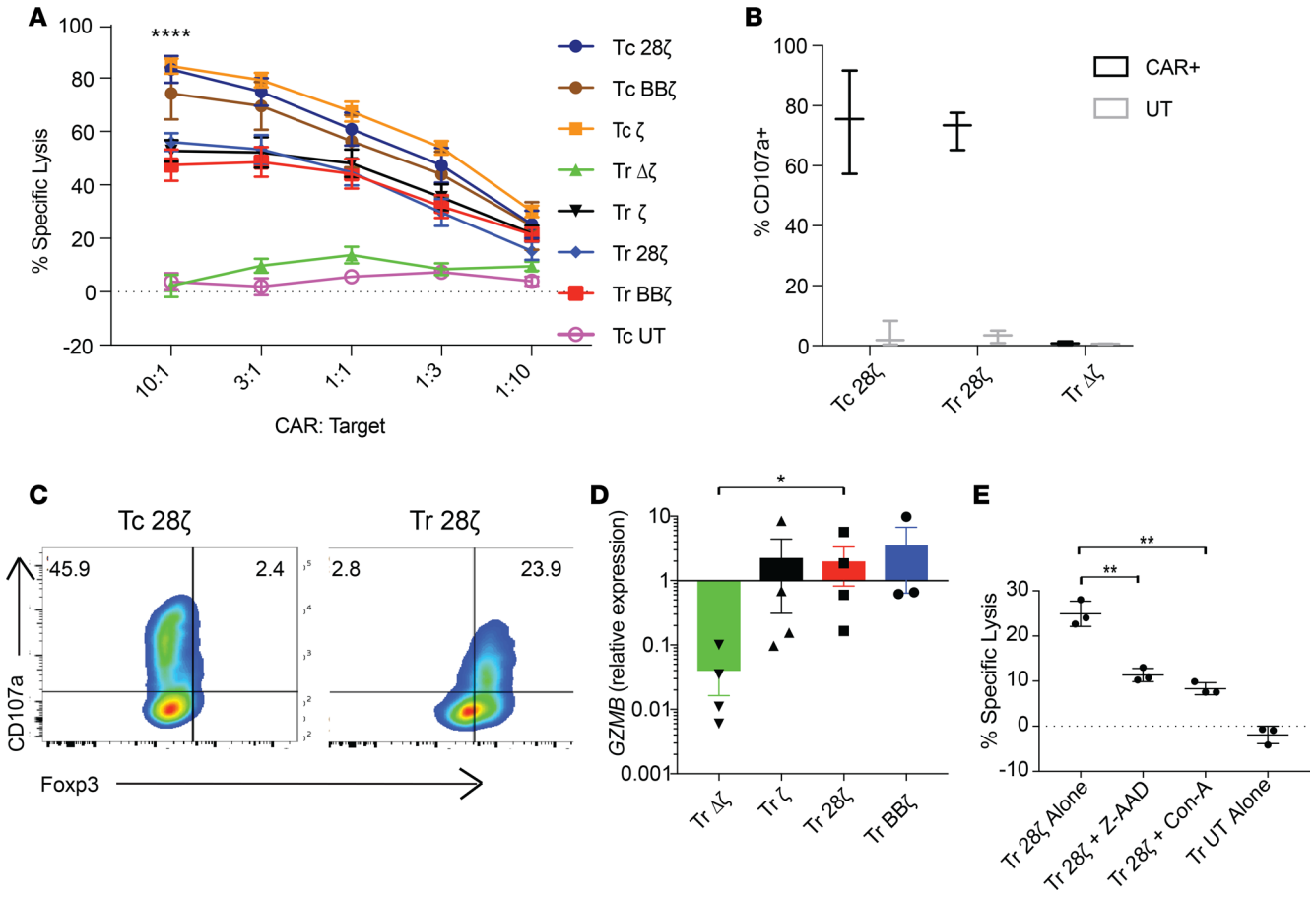

Figure 5. Foxp3⁺ CAR-Tregs degranulate and mediate target cell cytolysis. (**A**) Luciferase-based killing assay of CD19⁺ target cells (Nalm6 CBG-GFP) at indicated T cell–to-target ratios for 16 hours. ****$P < 0.0001$, by paired *t* test of Tconvs compared with Tregs (10:1 ratio, $n = 3$ human donors). (**B**) Whiskers plot depicting the percentage of CD107a⁺ of total mCherry⁺ (CAR) or mCherry⁻ (UT) cells over a 6-hour coculture with live Nalm6 cells measured on nonfixed cells by flow cytometry ($n = 3$ human donors). (**C**) After the 6-hour coculture with Nalm6 in the presence of CD107a antibodies, T cells were fixed, permeabilized, and stained for intracellular Foxp3. Representative donor flow plots of CD107a versus Foxp3. Data are representative of $n = 3$ human donors. (**D**) *GZMB* expression of sorted CAR-Tregs after 24-hour Nalm6 stimulation, measured by digital droplet PCR and expressed as a relative ratio to the internal control gene *TBP* ($n = 3$ human donors). (**E**) Luciferase-based killing assays of Nalm6 CBG-GFP with granzyme/perforin inhibitors CMA or Z-AAD-CMK added to the media (1:3 T cell-to-target ratio, 16-hour incubation time). Data are representative of 3 donors with technical triplicates (repeated with $n = 3$ human donors). Data represent mean ± SEM for **A**, **D**, and **E**. *$P < 0.05$, by paired *t* test comparing Tr Δζ and Tr 28ζ (**D**), and **adj-$P < 0.01$, by unpaired *t* test with Holm-Bonferroni method adjustment for 2 tests (**E**). Tc, Tconvs; Tr, Treg.

the consumption of IL-2 (44–46). Although IL-10–mediated suppression is rarely observed in vitro (47), we had observed differences in IL-10 secretion among CAR-Tregs; therefore, we repeated the proliferative suppression assay in the presence of established IL-10–blocking antibodies (48), but IL-10 blockade had no discernable effect (Supplemental Figure 3A). Next, we tested whether IL-2 consumption at rest and upon activation was different among various CAR-Tregs. We measured IL-2 in the media of CAR-Tconvs and CAR-Tregs after 40 hours in culture in the absence or presence of antigen. Tconvs did not consume IL-2 at baseline and secreted more IL-2 then they consumed after activation through the CAR (Supplemental Figure 3B), whereas CAR-Tregs consumed IL-2 at baseline and after activation, with BBζ CAR-Tregs consuming more IL-2 than 28ζ, ζ, and Δζ CAR-Tregs at baseline ($P = 0.0014$, BBζ to 28ζ, paired ratio *t* test) (Supplemental Figure 3C). However, BBζ CAR-Tregs did not significantly increase their consumption of IL-2 after antigen stimulation, whereas 28ζ CAR-Tregs significantly increased their consumption of IL-2 after antigen stimulation ($P = 0.004$, BBζ to 28ζ, paired ratio *t* test) (Supplemental Figure 3C). Furthermore, when we added excess rhIL-2 to the culture, Tregs lost their ability to suppress the proliferation of Tconvs, with no difference among the CAR-Tregs (Supplemental Figure 3D). These data suggest that antigen stimulation through CARs induces differential increases in consumption of IL-2 by CAR-Tregs that are important for their suppressive function.

CAR-Tregs degranulate and induce target cell cytolysis in vitro in a granzyme B–dependent mechanism. Although there has been interest in generating tissue-specific CAR-Tregs to protect the target tissue, we were concerned with the possibility that CAR-Tregs could also mediate antigen-specific lysis. CAR-modified $CD4^+$ Tconvs can kill antigen-expressing targets cells at similar efficiency to the classic cytotoxic $CD8^+$ T cell (49), and Tregs have also been reported to induce apoptosis in Teffs through granzyme B–mediated cytolysis (50–53). We therefore sought to determine whether CD19 CAR-Tregs would gain similar cytolytic function and induce apoptosis in cells expressing CD19. We measured cytotoxicity by titrating CAR-Tconvs and CAR-Tregs with $CD19^+$ target cells. We found that all functional CAR-Tregs killed their target cells, irrespective of their costimulation domain, but with a significantly lower efficiency than $CD4^+$ Tconvs (Figure 5A). Because the type of costimulation domain did not affect CAR-Treg cytotoxicity, we chose to only focus on the 28ζ CAR-Tregs to better understand this cytotoxicity. We confirmed that both CAR-Tconvs and- Tregs degranulated when incubated with $CD19^+$ targets (Figure 5B) or PMA/ionomycin (Supplemental Figure 4A) and did not degranulate in the absence of CAR or TCR stimulation (Supplemental Figure 4B). We also confirmed that antigen stimulation induced degranulation of both $FoxP3^-$ Tconvs and $FoxP3^+$ Tregs and that this was not due to contamination of the Treg cultures with Tconvs (Figure 5C). We performed digital droplet PCR to determine the expression levels of *GZMB*, *GZMA*, and *PRF1* (encoding proteins granzyme B, granzyme A, and perforin, respectively) in CD19 CAR-Tregs and -Tconvs after a 24-hour stimulation with $CD19^+$ target (Nalm6) cells. We found that *GZMB* was specifically upregulated in functional activated CAR-Tregs compared with Δζ Tregs (Figure 5D), though *GZMB* expression was not as high as in activated CAR-Tconvs (Supplemental Figure 5A). *GZMA* was not induced by CAR activation, and *PRF1* expression was similar across CAR-Tregs and -Tconvs (Supplemental Figure 5, B and C, respectively). Addition of perforin/granzyme B pathway inhibitors (with either concanamycin A, a perforin inhibitor, or Z-AAD-CMK, a granzyme B specific inhibitor) reduced both Treg (Figure 5E) and Tconv cytotoxicity (Supplemental Figure 5D). We also investigated whether sorting naive Tregs based on the positive expression of CD45RA would prevent target-specific cytolysis by Tregs. However, $CD45RA^+$ CAR-Tregs displayed equal cytolytic activity compared with bulk Tregs in the Nalm6/CD19 models (Supplemental Figure 5E).

Because second-generation CD28-containing CAR-Tregs directed to HLA-A2 were not reported as having cytotoxicity toward target cells in vitro (31, 32), we asked whether this cytotoxicity could be due to the high-affinity CD19 scFv binder in our CARs. To test this hypothesis, we generated a first-generation CAR with an scFv against EGFRvIII (EGFRvIII-ζ, Supplemental Figure 6A), which is known to have a significantly lower affinity to its cognate antigen than the CD19 scFv (EC_{50} of ~6 ng vs. ~100 ng) (54, 55). We transduced U87 glioblastoma target cell lines to express either CD19 or EGFRvIII antigens. We confirmed that first-generation EGFRvIII CAR-Tregs can suppress antigen-specific CAR-Teff proliferation when activated with $EGFRvIII^+$ U87 cells (Supplemental Figure 6B). Despite the lower-affinity scFv, we found that EGFRvIII CAR-Tregs induced target specific cytolysis (Supplemental Figure 6C) and degranulation (Supplemental Figure 6D), similar to CD19-specific CAR-Tregs incubated with $CD19^+$ U87 cells (Supplemental Figure 6E). In conclusion, both peripheral and naive CAR-modified Tregs display target cell–specific lysis in vitro — albeit less than Tconvs — that is independent of the affinity of the scFv and is at least partly dependent on the granzyme B/perforin pathway.

In vivo models of CAR-Treg accumulation and cytotoxicity. To test whether CAR-Tregs accumulate specifically at sites expressing their CAR target in vivo, we injected NSG mice with $CD19^+$ or $CD19^-EGFR^+$ U87 cell lines s.c. into the left and right flank, respectively. One week after tumor injection, we injected the mice i.v. with CD19-directed 28ζ CAR-Tregs. Mice were administered 8 μg/mouse rhIL-2 via intraperitoneal injections 3 times a week from day 0, which was necessary to support Treg survival in vivo in the absence of IL-2–secreting Teffs (47, 56–58). Tumors were harvested at day 14 and examined histologically for tumor necrosis as an indicator of T cell–mediated lysis and the presence of CAR-T cells as an indicator of T cell accumulation (Figure 6A). We found anti-CD19 28ζ CAR-Tregs accumulated specifically in the U87-CD19-expressing tumor, whereas we did not observe their presence in the U87-$CD19^-$ tumor (Figure 6B). We did not observe any antitumor activity in CAR-Treg–treated mice (data not shown). We hypothesized that if Tregs were to cause low levels of target specific destruction, it would be more relevant and observable in a nontumor model, where the target cells are not able to proliferate at the rapid rate of tumor cells. Therefore, we developed a skin xenograft model where NSG mice were grafted with human skin that endogenously expresses EGFR and which we have previously used to measure EGFR-directed

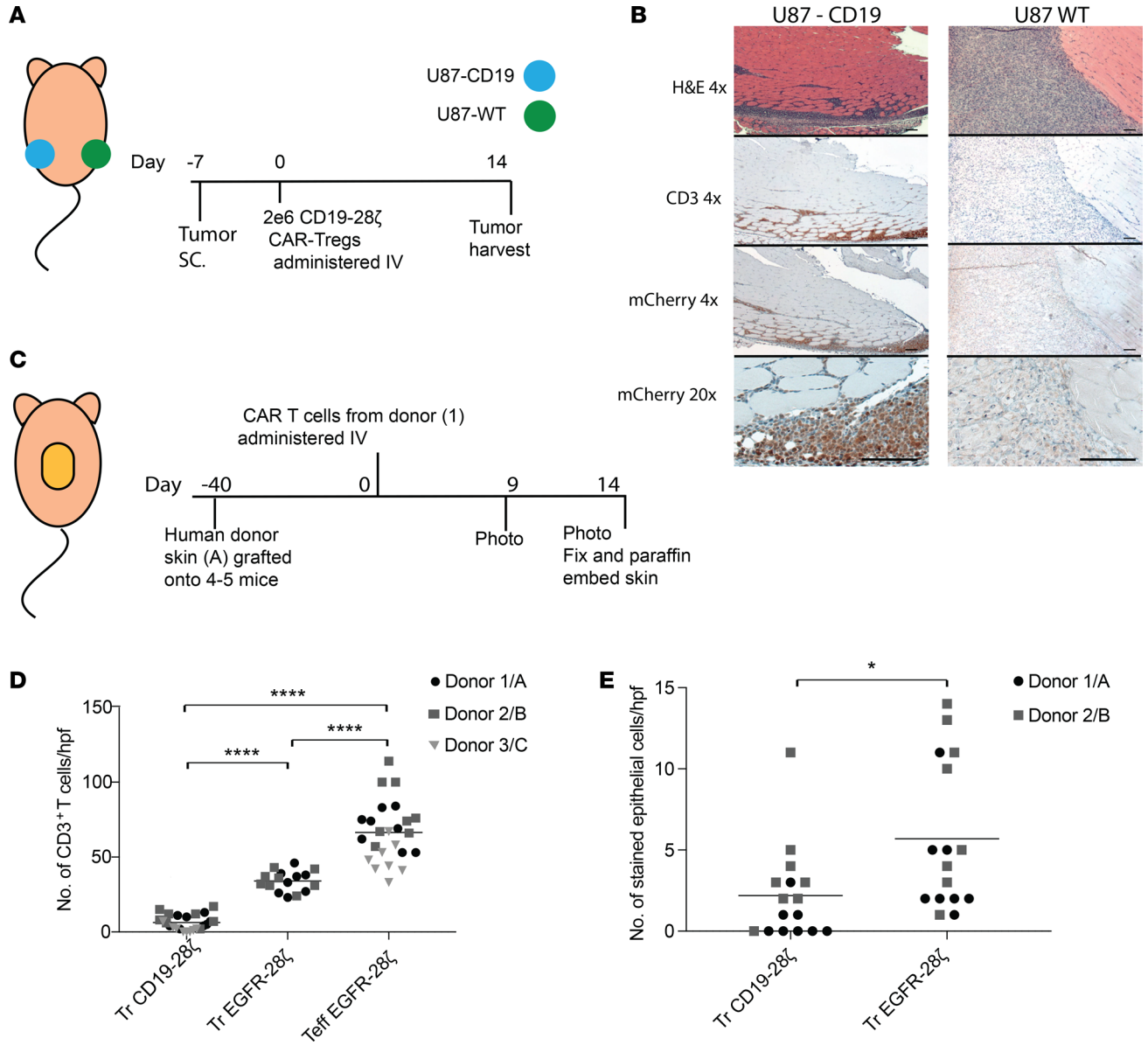

Figure 6. CAR-Tregs accumulate in antigen-expressing tissue in vivo. (**A**) U87 s.c. tumor model for CAR-Treg trafficking experimental outline. U87 WT, WT U87 cells (EGFR$^+$CD19$^-$); U87-CD19, U87 cells transduced with CD19. (**B**) Representative images of H&E, CD3, and mCherry immunohistochemical staining of U87-CD19 and U87-WT tumors from mice treated with CD19-28ζ CAR-Tregs. Scale bar: 100 μm. (**C**) Skin xenograft model experimental outline. For each experiment, several mice were grafted with skin from the same human donor (i.e., graft, donor A, B, or C) and then were treated with T cells all derived from a single donor leukopacks (i.e., T cell donor 1, 2, or 3). (**D**) T cells were quantified from CD3 IHC-stained graft sections in areas just below the dermal/epidermal junction. The number of cells were counted per high-power field (hpf; original magnification, ×400). (**E**) TUNEL$^+$ cells in the epidermis along the dermal/epidermal junction were quantified/hpf (original magnification, ×2000. $n \leq 2$ repeats with different donor skin and donor T cells/experiment). ****adj-$P < 0.0001$, by 1-way ANOVA with Tukey's multiple comparisons test (**D**), and *$P < 0.05$, by paired t test with donors combined (**E**).

toxicity and graft rejection with CAR T cells (55). After the skin grafts had healed, we injected EGFR-28ζ CAR-Tregs or EGFR-28ζ CAR-Teffs as a positive control (Supplemental Figure 7, A and B). Grafted mice injected with CD19-28ζ CAR-Tregs were included as a control for antigen specificity. Mice receiving Tregs were administered rhIL-2 to allow Treg survival in vivo as described above. The mice were monitored and the skin grafts photographed over 2 weeks; grafts were harvested for histology at day 14 (Figure 6C). We observed T cell infiltration into the skin grafts of mice that received either EGFR CAR-Tregs or CAR-Teffs, though greater numbers of Teffs than Tregs accumulated in the grafts (Figure 6D). In contrast, we could not detect CD19 CAR-Tregs in the skin graft, again demonstrating the antigen-specific nature of CAR-Tregs. TUNEL staining of the graft sections showed minimal but observable keratinocyte death

in the EGFR CAR-Tregs compared with the CD19 CAR-Tregs (Figure 6E and Supplemental Figure 7C), but this was minimal compared with the grafts of mice that had received EGFR CAR-Teffs; these grafts were rejected to the extent that there was no remaining epidermis within which to quantify the TUNEL$^+$ cells. Nevertheless, there were more TUNEL$^+$ cells in the remaining dermis of Teff-treated mice than in the Treg-treated mice (Supplemental Figure 7C). Thus, we found that CAR-Tregs alone can mediate very low but measurable cytotoxicity against tissues expressing the target antigen.

CD28-containing CAR-Tregs suppress Teffs in vivo. Because the tissue damage by CAR-Tregs was minimal, we then tested EGFR CAR-Tregs for their ability to suppress the damage caused by EGFR CAR-Teffs in the same skin xenograft model. To this end, we set up a similar experiment but included an additional test group in which EGFR-28ζ CAR-Teffs were administered in combination with EGFR-28ζ CAR-Tregs at equal ratios. Indeed, the grafts of the mice that received Teffs alone contracted in size and showed clear signs of rejection (Figure 7A and Supplemental Figure 7D). However, in mice treated with the same number of Teffs in combination with EGFR-28ζ CAR-Tregs, the graft did not contract and there was no observable skin rejection (Figure 7A). By histopathology, graft rejection was obvious in the Teff-treated graft, with dense lymphocyte infiltration, spongiosis, and exocytosis of the epidermal layer. In some areas, the epithelium had been destroyed and there were signs of epithelial apoptosis, dyskeratosis, and keratinolysis (Figure 7B). In contrast, when EGFR-28ζ CAR-Tregs were coadministered with Teffs, there were no signs of epithelial destruction or graft rejection, indicating that in vivo the CAR-Treg suppressive function was dominant over Teff rejection. IHC staining for mCherry confirmed that the T cells infiltrating the grafts were indeed CAR T cells (Figure 7B). Foxp3 IHC staining revealed that the mice treated with EGFR CAR-Tregs alone or in combination with Teffs had nuclear Foxp3 staining of some of the cells, whereas the grafts treated with Teffs only had only rare Foxp3$^+$ cells in the graft (Figure 7B and Supplemental Figure 7E). Finally, IHC and quantification of the number of CD8$^+$ T cells present in the graft indicated that the presence of EGFR-28ζ CAR-Tregs decreased the number of CD8$^+$ T cells in the graft (Figure 7C). This observation held true over individual and pooled multiple experiments with T cells from 3 different donors (donors 1, 2, and 3) tested against skin grafts from 3 different donors (donors A, B, and C).

To investigate potential mechanisms of CAR T cell suppressive functions in the grafts, we used RNAscope to measure *IL10* and *TGFB1* (encoding immunosuppressive cytokines IL-10 and TGF-β, respectively) as well as *GZMB* and *PRF1*. We found the presence of *IL10* and *TGFB1* RNA expression in the grafts with CAR-Treg alone, and their expression was also greatly increased in grafts from mice administered the combination of EGFR CAR-Tregs with CAR-Teffs (Figure 8A). In contrast, *GZMB* and *PRF1* were expressed at the highest levels in grafts treated with Teffs alone but at a lower level in the Teffs with Treg-treated grafts (Figure 8A). We did not detect significant levels of *PRF1* or *GZMB* expression in mice treated with EGFR CAR-Tregs alone or CD19 CAR-Treg–treated mice (Figure 8A).

Finally, we asked whether the decrease in BBζ CAR-Treg suppressive function that we had observed in vitro was also reflected in vivo. We grafted 3 mice with skin from a single human donor (donor C or D), and once the grafts had healed, we injected the mice with EGFR-28ζ Teffs alone or in combination with either EGFR-28ζ or EGFR-BBζ CAR-Tregs, with T cells derived from 1 donor (donor 3 or 4). Once again, by histology and TUNEL staining, EGFR-28ζ CAR-Tregs decreased the cell death and destruction of the epidermis by antigen-specific Teffs. However, EGFR-BBζ CAR-Tregs were unable to prevent destruction of the epidermis, and we detected significantly more TUNEL staining in the dermis of the grafts treated with Teffs in combination with BBζ Tregs compared with 28ζ Tregs (Figure 8, B and C), confirming our in vitro results of reduced suppressive capacity of BBζ CAR-Tregs.

Discussion

Analogous to the use of conventional CAR T cells as adoptive immunotherapy for cancer, we and others have found that transduction of Tregs with lentiviral vectors coding for CARs endows Tregs with new antigen specificity. Antigen-specific or tissue-specific Tregs have enormous therapeutic potential for GvHD, generating transplant tolerance and preventing or reversing tissue-specific autoimmunity. Although the effects of CAR-encoded costimulation domains have been described in CAR Tconvs (23), the varying effects of these domains have not been described in Tregs. We found that the costimulation domains we tested do not affect the expression or methylation status of transcription factor Foxp3 in Tregs. We confirmed that Tregs suppress antigen-specific T cell proliferation and cytokine secretion but

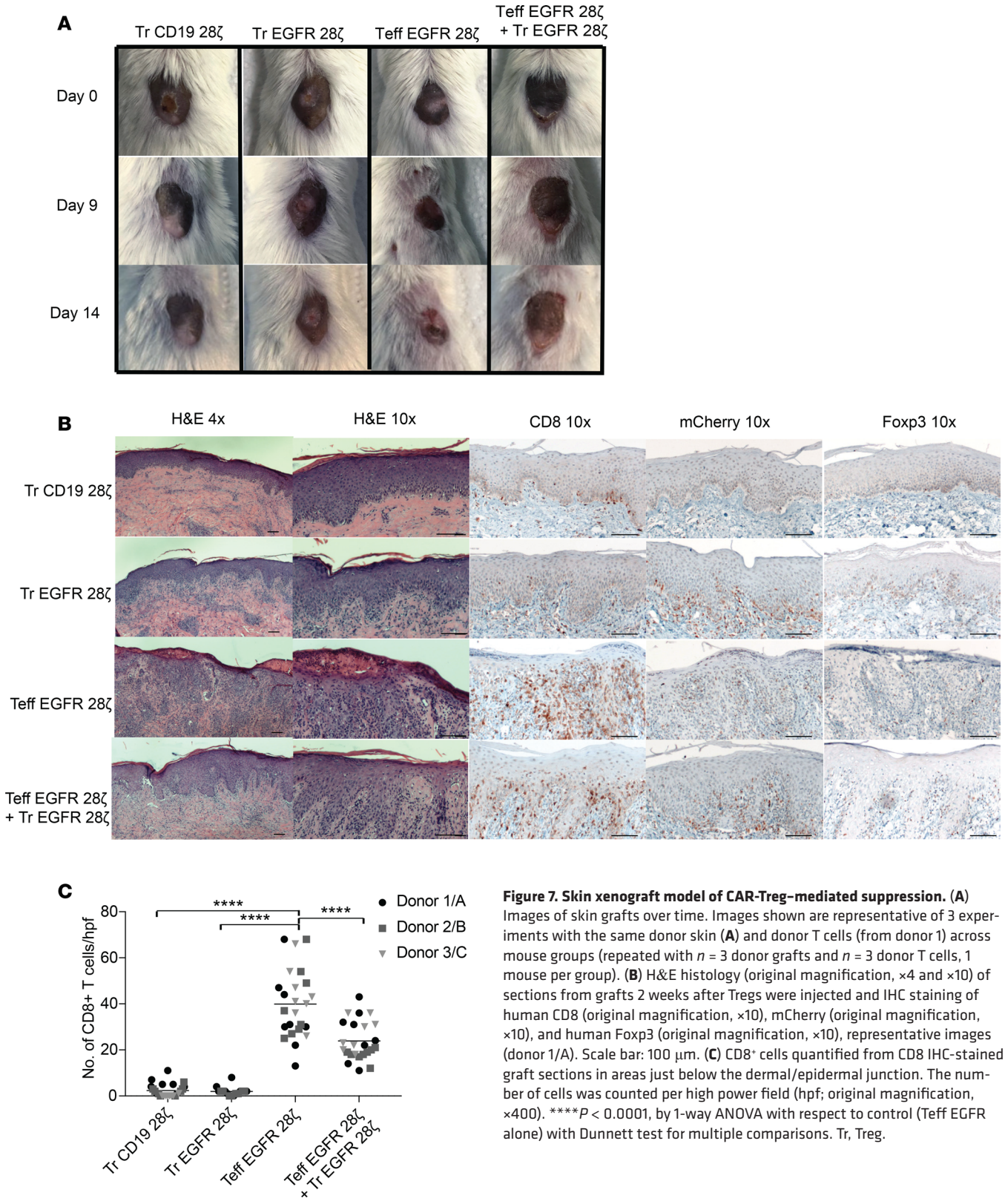

Figure 7. Skin xenograft model of CAR-Treg–mediated suppression. (**A**) Images of skin grafts over time. Images shown are representative of 3 experiments with the same donor skin (**A**) and donor T cells (from donor 1) across mouse groups (repeated with $n = 3$ donor grafts and $n = 3$ donor T cells, 1 mouse per group). (**B**) H&E histology (original magnification, ×4 and ×10) of sections from grafts 2 weeks after Tregs were injected and IHC staining of human CD8 (original magnification, ×10), mCherry (original magnification, ×10), and human Foxp3 (original magnification, ×10), representative images (donor 1/A). Scale bar: 100 μm. (**C**) $CD8^+$ cells quantified from CD8 IHC-stained graft sections in areas just below the dermal/epidermal junction. The number of cells was counted per high power field (hpf; original magnification, ×400). $^{****}P < 0.0001$, by 1-way ANOVA with respect to control (Teff EGFR alone) with Dunnett test for multiple comparisons. Tr, Treg.

found that the costimulation domain could modulate the suppressive functions of the Tregs specifically when stimulated through the CAR.

Previous research has shown that the addition of 4-1BB ligand (4-1BBL) abrogates Treg suppression in standard coculture assay, but this was largely believed to reflect a role for 4-1BB signaling in allowing Teffs

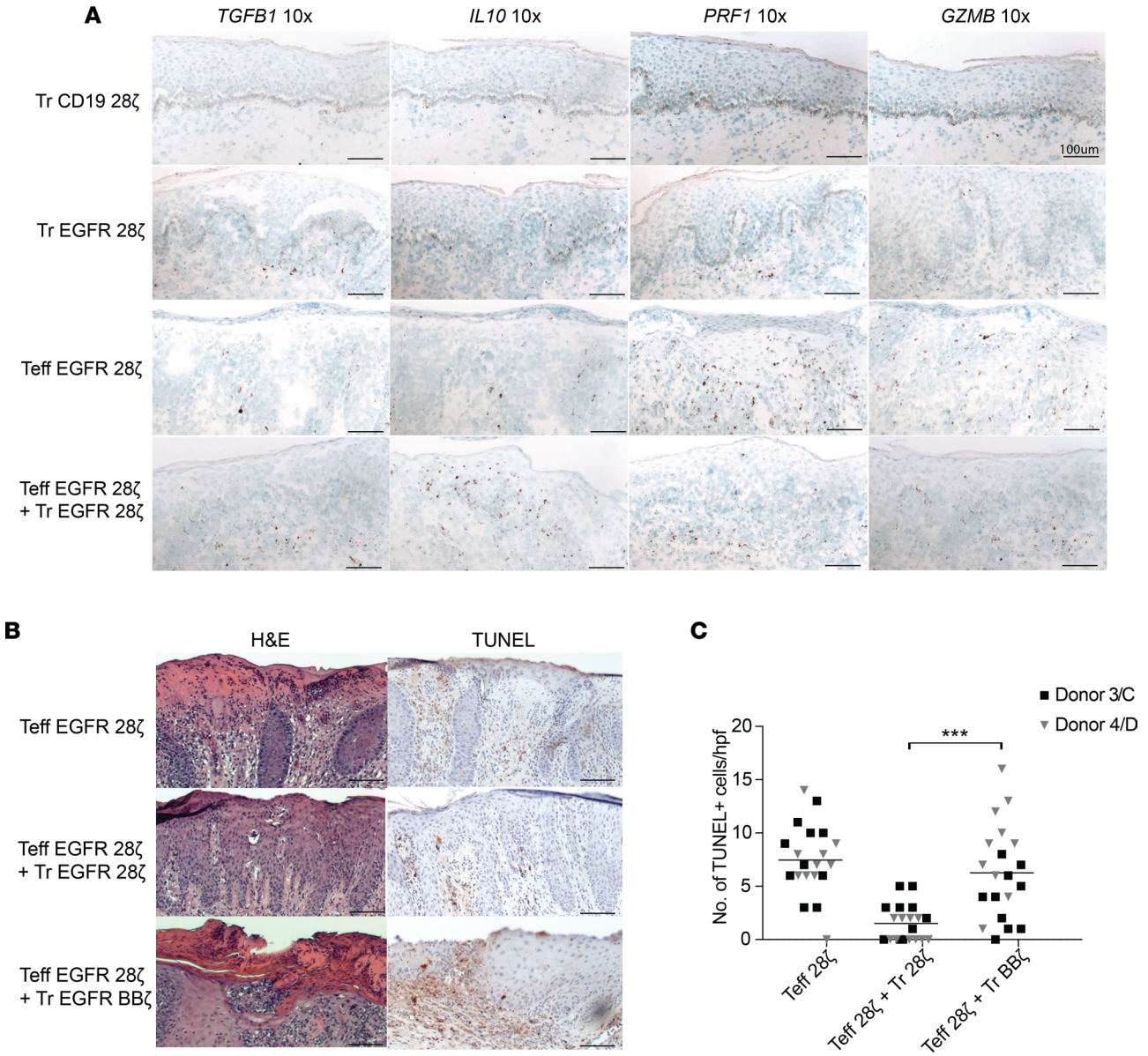

Figure 8. CAR-Tregs express immunosuppressive cytokines in vivo. (**A**) Representative images of RNAscope staining of *TGFB1* (original magnification, ×10), *IL10* (original magnification, ×10), *PRF1* (original magnification, ×10), and *GZMB* (original magnification, ×10) mRNA (donor 1/A). (**B**) Representative images of H&E and TUNEL staining (original magnification, ×10) of skin xenografts from mice after treatment with combinations of CAR-Tregs and CAR-Teffs (donor 4/D). Scale bar: 100 μm. (**C**) TUNEL$^+$ cells in fields viewed directly below the dermal/epidermal junction quantified/hpf (original magnification, ×400). ***$P < 0.001$, by paired *t* test between Teff with Tr 28ζ versus Teff with Treg BB. Tr, Treg.

to become resistant to suppression rather than by direct impairment of Treg function (37). However, our data suggest that the 4-1BB signaling may trigger both the direct suppression of Treg function and the provision of costimulation to Teffs that reduces susceptibility to Treg suppression. Others have shown that 4-1BB costimulation increases Treg expansion (59). We speculate that the ability of a Treg to proliferate does not correlate with the ability of a Treg to suppress immune responses, as we also did not observe changes in Treg expansion in vitro. Another possibility is that there is a difference in signal strength and kinetics between physiological 4-1BBL receptor signaling in Tregs versus CAR-mediated 4-1BB costimulation. The constitutive nature of CAR expression may not fully replicate the coordinated signaling of temporally expressed 4-1BB receptor, which occurs several hours after activation through the TCR.

We found other indicators that CD28 costimulation was more beneficial than 4-1BB costimulation to Tregs in terms of maintaining their Treg phenotype functions. For example, CAR 28ζ Tregs expressed more LAP and CTLA4 than BBζ CAR-Tregs, and CAR-mediated activation led to greater production of IL-10 in

28ζ Tregs than BBζ CAR-Tregs. In addition, IL-2 consumption increased more in 28ζ Tregs when activated through their CAR. Tregs are hypothesized to suppress Teffs through the combination of several of these and other mechanisms (44, 52). The effect of each one of these differences between 28ζ and BBζ alone may not have an observable effect on Treg function but, in combination, results in reduced antigen-specific suppression of Teffs by BBζ CAR-Tregs.

Another aspect of Treg suppression to consider is that Tregs suppress Teffs both directly and indirectly through their regulation of APCs in secondary lymphoid tissues, spatially separated from the target tissue. Our research focused on the direct effect of Treg suppression on Teffs, though it would be interesting to see if the same differences between CD28 and 4-1BB costimulation would be observed where indirect suppression by Tregs is also considered. However, testing these hypotheses would require immunocompetent mice with intact APCs and secondary lymphoid organs, and probing questions about the function of human T cells would no longer be feasible. Furthermore, the clinical use of CAR-Tregs in patients would more likely mimic our experimental setup, where the cognate antigen of the CAR is expressed by the tissue requiring protection. We do recognize and acknowledge that the CAR-Treg on CAR-Teff model is contrived, given that CAR-Tregs would not be used clinically to suppress CAR-Teffs; however, we found it to be the only reproducible method to demonstrate antigen-specific CAR-Treg functions, where antigen-specific refers to triggering of the CAR. Given that one of our early findings was that CAR-Tregs could be cytotoxic, we considered several in vivo models in which to test our CAR-Tregs. Because a GvHD model would not be able to distinguish cytotoxic effects from suppressive effects of Tregs, we specifically sought a normal tissue model to evaluate which effect was dominant in CAR-Tregs with different signaling domains. To this end, we determined that a skin graft model would allow evaluation of either effect in one tissue and had the greatest potential of extending the in vitro studies.

Activation of Tregs induces bystander suppression of other inflammatory cells in the vicinity (15). Therefore, we postulate that it is not necessary to know the antigens activating autoreactive T cells in order to broadly suppress inflammatory immune cells at a tissue site of inflammation. In fact, directly targeting the cell that requires protection from effector T cells may not be the best strategy, given the low-level cytolytic activity of CAR-Tregs. Instead, we would propose targeting CAR-Tregs to a nonessential cell type capable of regeneration but that could recruit CAR-Tregs to that tissue and exert a "zone" of immunosuppression. Here, we found that CD19 CAR-Tregs and EGFR CAR-Tregs both accumulated specifically in antigen-expressing tissues in vivo; although minimal tissue damage was observed in vivo, we remain cautious about the use of CAR-Tregs that directly target an essential nonregenerating cell type, such as neurons or cardiomyocytes.

The common occurrence of B cell aplasia highlights the damage that anti-CD19 scFv CAR T cells can inflict on normal tissues that express the target antigen (60). Therefore, as CAR-Tregs move toward the clinic, understanding the potential for tissue destruction is critical. One way to minimize potential on-target toxicity would be to design CARs against secreted or soluble antigens, such that the CAR cannot form a synapse with a cell that can be lysed. Other possibilities could include modifying CAR-Tregs further by knocking out genes important for their cytotoxicity, such as GZMB. It is interesting that others have not reported the cytotoxicity we found in our in vitro assays (31, 32), though Treg-mediated lysis of APCs expressing MHC class II with peptide is thought to be one mechanism by which Tregs induce tolerance. Perhaps one reason for this observation is that we cultured Tregs in the absence of rapamycin, and rapamycin inhibits granzyme B production (61).

In summary, we identified 3 unexpected findings in the field of CAR-Treg therapy: first, incorporation of the 4-1BB signaling domain in CAR-Tregs reduces their immunosuppressive function, whereas first-generation or CD28 costimulation maintains phenotypic stability and immunosuppressive function of human Tregs; second, CAR-Tregs can accumulate at the sites of antigen expression in vivo and exert functional immunosuppression against large numbers of Teffs that would otherwise destroy the target tissue; and third, CAR-Tregs may exert minimal levels of antigen-specific cytotoxicity on their own, regardless of scFv affinity, suggesting that a cautious approach is warranted in clinical trials of CAR-Tregs directed to life-sustaining tissues. Nevertheless, CAR transduction of Tregs overcomes several obstacles previously inherent to Treg therapy and holds promise for antigen-specific immune suppression in a variety of settings.

Methods

Cell isolation. CD4$^+$ T cells were negatively selected from healthy donor leukopacks using CD4 T cell enrichment RosetteSep Kits with a Ficoll gradient (Stemcell Technologies) and enriched for CD25$^+$ cells using CD25-PE antibody staining followed by anti-PE microbead selection according to the manufacturer provided protocol (Miltenyi). T cells were stained separately at 4 × 10^6 cells/100 μl, for 30 minutes at 4°C in PBS with 50 μl/100 μl brilliant violet staining buffer (BioLegend), 5 μl/100 μl CD127-BV711, 5 μl/100 μ CD4-BV510, and 2.5 μl/100 μl CD8-APC-H7. Stained cells were washed and resuspended in HBSS supplemented with 25 mM HEPES and 1% FBS with DAPI prior to sorting. Tregs were purified from CD25-enriched cells by FACS and selected as live CD4$^+$, CD8$^-$, and CD25^{++}CD127^{lo} cells and collected in 50% FBS in PBS. Tconvs were sorted from CD25-depleted cells by selecting for live CD4$^+$CD8$^-$CD25^{lo} cells and collected in 50% FBS in PBS. Nonenriched cells were used to draw the CD25^{++} sorting gates that we defined as the level of CD25 expression where a shift to slightly lower for CD4 staining could be seen. For experiments using bulk CD4$^+$CD8$^+$ T cells, cells were negatively selected as described above with the T cell enrichment RosetteSep kit (Stemcell Technologies).

In vitro cell culture. Tregs and Tconvs were then expanded with anti-CD3/anti-CD28 beads (Dynabead Human Treg expander or Dynabead Human T-activator beads, respectively, Gibco) in CTS OpTmizer T Cell Expansion Serum Free Media (Thermo Fisher Scientific) supplemented with 2% human serum (Access Cell Culture LLC), 1× GlutaMAX (Thermo Fisher Scientific), 100 U/ml penicillin-streptomycin (Thermo Fisher Scientific), and recombinant human IL-2 (used at 300 IU/ml for Tregs and 20 IU/ml for Tconvs, Peprotech). One day after sort, T cells were transduced at an MOI of 5 with lentivirus carrying one of the 5 CAR constructs with a humanized scFv that binds human CD19 and intracellular domains: 4-1BBζ, CD28ζ, ζ, and Δζ followed by a T2A and mCherry. T cells were expanded for 1 week with beads and then debeaded and rested for another week. Media was added every 2–3 days to maintain cells at a concentration of 1 × 10^6 to 2 × 10^6 T cells/ml. IL-2 was replaced every 2–3 days.

Cell lines. Human embryonic kidney 293 (HEK293T), K562, U87, and Nalm6 cell lines were purchased from ATCC. HEK293T, K562, and Nalm6 cells were expanded in R10. U87 cells were grown in Eagles minimum essential media (ATCC) supplemented with 10% FBS. Cell lines were routinely tested for mycoplasma and contamination was never detected.

Construct generation and lentivirus production. CD19-, EGFRvIII-, and EGFR-specific CARs were synthesized and cloned into a third-generation lentiviral plasmid backbone under the regulation of a human EF-1α promoter (GenScript USA Inc). Replication-defective lentiviral vectors were produced by 4 plasmids cotransfected into HEK293T cells using TransIT-2020 transfection reagent (Mirus). Supernatants were collected 24 and 48 hours after transfection. Virus was filtered and then concentrated by ultracentrifugation. Vector was harvested and stored at –80°C.

Flow cytometry reagents and analysis. Fluorescent anti-CD3 (OKT3), anti-CD4 (OKT4), anti-CD8 (SK1), anti-CD69 (FN50), anti-LAP (TW4-2F8), anti-CD137 (4B4-1), and anti-CTLA4 (L3D10) antibodies were purchased from Biolegend. Anti-CD25 (2A3), anti-CD127 (HIL-7R-M21), and anti-CD107a (H4A3) fluorescent antibodies were purchased from BD Biosciences. Fluorescent anti-CD39 [eBioA1(A1)] and anti-LAG3 (CD223, 3DS223H) were purchased from eBioscience. For Foxp3 intracellular staining anti-Foxp3 (PCH101) antibodies were purchased from eBioscience. After surface staining, T cells were fixed and stained with the eBioscience Foxp3 transcription factor staining kit, as described in the Supplemental Methods.

DNA methylation analysis. 5 × 10^5 Tregs and Tconvs were sorted by CD3 and mCherry expression, except in the case of UT T cells, which were sorted on CD3 only. Sorted cells were then washed in PBS and snap frozen before shipment to EpigenDx for methylation analysis. The methylation status of CpG motifs across the *FOXP3* TSDR, *CTLA4*, and *IKZF2* loci was assessed by targeted next-generation bisulfite sequencing using the EpigenDx Human Foxp3 methylation panel. The percentage of methylation at each CpG site was averaged and then represented as an average from 2–3 human donors/group; only female donors were used for TSDR methylation analysis.

T cell assay overview. Assays were performed on never-frozen Tregs on day 14–15 in either supplemented OpTmizer media or RPMI-1640 with 1× GlutaMAX and 25 mM HEPES (Gibco, Life Technologies) supplemented with 10% FBS and 100 U/ml penicillin-streptomycin (R10) as stated. For all assays, CAR T cells were normalized to the same percentage of CAR$^+$ cells by adding appropriate numbers of expanded UT Treg or Tconvs. All experiments were performed with CAR transduction above 50%.

TCR versus CAR restimulation. Assays were performed in supplemented OpTmizer media. For methylation and phenotypic and proliferation analysis of long-term activated CAR T cells, 1×10^6 CAR-Tregs or CAR-Tconvs were stimulated with irradiated K562 cells expressing surface anti-CD3 scFv (OKT3) or CD19 at a 1:1 T cell–to-target ratio in a 12-well plate. Cells were maintained in culture at a concentration of 5×10^5 to 2×10^6 cells/ml. T cells were counted using a LUNA-FL dual-florescence cell counter (Logos Biosystems) and analyzed by flow cytometry every 2 days for 8 days to account for live K562 cells in the culture, while documenting the expansion of T cells. For phenotypic analysis, surface and intracellular staining for markers CD39, CTLA4, LAP, and Foxp3 was measured by flow cytometry before (day 14) and 9 days after (day 23) K562 stimulation. For methylation analysis, T cells were also sorted by $mCherry^+$ and $CD3^+$ and then frozen at –80°C for DNA methylation analysis.

For short-term (24-hour) activation assays, Tregs were grown in reduced IL-2 media (20 IU/ml) from day 12–14. On day 14, 1×10^5 T cells/well were activated in a 96-well round-bottom plate at 1×10^6 CAR T cells/ml with either no target cells or at a 2:1 T cell–to-target ratio with irradiated K562-CD19 or K562-OKT3 cells in a final volume of 200 μl/well in technical triplicates. Cells were incubated at 37°C for 24 hours. Triplicate wells were pooled and stained for CD3, CD4, CD69, LAP, and 4-1BB (CD137), and surface expression was measured by flow cytometry. In duplicate experiments, supernatants from stimulated T cells were frozen followed by cytokine detection by luminex, as described in the Supplemental Methods.

Suppression assays. Tregs were violet-labeled as described in Supplemental Methods and used in MLRs with CFSE-labeled Teffs (following the same protocol for violet labeling, CFSE cell trace, Invitrogen, 1 M staining concentration). Tregs were titrated in a 96-well plate with 5×10^4 Teffs/well and 1×10^5 irradiated target cells/well in R10. Cells were left in an incubator at 37°C for 3–4 days, unless otherwise noted, with 100 μl media added on day 2. For cases in which beads were used for the proliferation assay, anti-CD3/anti-CD28 beads (Human T-activator beads, Dynabead) were used at a 1:10 bead-to-Teff ratio. To analyze MLR suppression assays, cells were stained with CD3-APC and CD8-APC-Cy7 for 30 minutes at 4°C and DAPI was added prior to flow cytometry on a Fortessa x-20 with a high-throughput plate reader. The percentage of suppression by Tregs in any condition (x) was calculated as the percentage of 1 – ($CFSE^{lo}$ cells of the total $mCherry^+$ $CFSE^+$ [$violet^-$] Teffs in condition [x] of the number of $CFSE^{lo}$ cells of $mCherry^+$ $CFSE^+$ Teffs in the no-Treg condition). Experiments were run in technical triplicates.

Cytokines from MLRs were measured from 50 μl supernatant using the luminex assay, as described in the Supplemental Methods. For IL-10–blocking assays, IL-10 antibody (LEAF purified, clone JES3-19F1, Biolegend) was added to wells at a final concentration of 10 μg/ml. For the MLR experiments with exogenous IL-2, rhIL-2 was added at a concentration of 50 IU/ml during plating and IL-2 was replaced when 100 μl media added on day 2.

Cytotoxicity assays. Luciferase-based killing assays were performed with CAR-Tregs and Tconvs as described previously (62). For the inhibition of granzyme/perforin pathways, we used granzyme-perforin axis inhibitor, concanamycin A (CMA; 200 nM, MilliporeSigma), and granzyme B–specific Inhibitor I (Z-AAD-CMK, 50 μM, Calbiochem). Inhibitor concentrations were chosen based on previously published studies investigating cytotoxicity by granzymes (53). Prior to use, each inhibitor was found to have insignificant effects on the viability of Tregs following an 18-hour incubation at 37°C, as assessed by a LUNA-FL dual-florescent counter. In inhibitor assays, all samples, including the target-alone samples, were incubated with the inhibitor to account for the effects of the inhibitor on tumor cell viability. Assays were run in technical triplicates.

In vivo mouse models. CAR T cells for in vivo experiments were isolated, expanded, and rested over 14 days, as described for the in vitro T cell assays. CAR T cell groups were normalized to have the same percentage of CAR on the day of administration in vivo.

For U87 tumor models, 8-week-old female NOD.Cg-*Prkdc*^{skid} *IL2rg*^{tm1wjl}/Szj (NSG) mice (The Jackson Laboratory) were injected on day –7 s.c. with 6×10^5 U87 CBG-GFP on the left flank and 6e5 U87-CD19 GBG-GFP on the right flank. 2×10^6 CAR T cells or the same number of UT T cells were injected i.v. on day 0, with 5 mice/group. In the groups where Tregs were given alone (without Teffs), recombinant human IL-2 was administered to the mice 3 times weekly at 8 μg/mouse via intraperitoneal injection. Tumor burden was regularly monitored using an Ami spectral imaging apparatus and analyzed with IDL software v. 4.3.1 following an i.p. injection of D-Luciferin substrate solution (30 mg/ml) 2 times a week. Animals were euthanized as per the experimental protocol. U87 tumors were removed on day 14 after CAR injection for paraffin embedding.

For skin xenograft models, human skin samples were obtained and harvested at the depth of the dermal boundary using a standard DermaBlade (Medline) and washed in RPMI media. NSG 8- to 10-week-old male mice were handled using standard aseptic technique. Mouse skin on the dorsum that was approximately twice as large as the graft was removed, immediately followed by creating micro wounds to the fascia using forceps to aid skin engraftment. The human donor graft was then secured to the mouse with silk ligature followed by sterile dressing. After 7–10 days, the sutures were removed and antibiotic ointment was applied to the grafts 3 times a week until grafts were fully healed. Once healed, approximately 30–60 days after surgery, mice were injected i.v. (day 0) with 2×10^6 CAR-Tregs, 2×10^6 CAR-Teffs, or both (4×10^6 CAR T cells total). Skin and donor T cells came from different human donors, but all mice in an experiment had skin grafts from the same donor (donors A–D) and received CAR T cells from the same donor (donors 1–4). In the groups where CAR-Tregs were given alone, IL-2 was administered i.p. at 8 μg/mouse 3 times weekly to allow the survival of Tregs in vivo. Grafts were photographed 3 times a week. Mice were euthanized on day 14, and tissue was harvested and fixed for paraffin embedding. Graft surface area was measured from images using SketchAndCalc software. Histology and RNA in situ hybridization were performed on the embedded tissues as described in the Supplemental Methods.

Statistics. Data are presented as mean ± SEM, as stated in the figure legends. Box-and-whiskers plots depict the medium and interquartile ranges (box) and minimum and maximum values (whiskers). Unless otherwise noted, groups were compared using a 2-tailed paired Student's *t* test. $P < 0.05$ was considered statistically significant unless adjustments for multiple corrections were needed, in which case adjusted P (adj-P) < 0.05 was considered significant. Holm-Bonferroni method was used to adjust P values from multiple comparisons across grouped paired data. One-way ANOVA comparisons were used with post-hoc Tukey or Dunnett test if $P < 0.05$, as stated. Statistical analyses were performed with Prism software version 7.0 (GraphPad), and Holm-Bonferroni adj-P were calculated with R software package (https://www.r-project.org).

Study approval. Healthy donor leukopacks were obtained from Blood Transfusion Services at Massachusetts General Hospital under a Massachusetts General Hospital IRB-approved protocol. Human skin was obtained from Massachusetts General Hospital according to a Massachusetts General Hospital IRB-approved protocol. All subjects provided written informed consent for the use of their discarded tissues for research. Tumor and xenograft procedures were performed as outlined in US and Massachusetts General Hospital Institutional Animal Care and Use Committee–approved requirements.

Author contributions

ACB and MVM designed the study. ACB, RCL, BDC, AAB, LSR, ASK, and ES performed experiments. ACB, SD, BRB, and MVM analyzed and interpreted data. CLC and DT provided critical reagents. ACB and MVM and wrote the manuscript. All authors edited and approved of the manuscript.

Acknowledgments

MVM was supported by NIH grant K08 CA166039, Stand Up to Cancer, the Damon Runyon Cancer Research Foundation, and grants from the Massachusetts General Hospital. ACB was supported by NIH grant 5T32AI118692-02. BRB was supported by NIH grant R01 HL11879. We would like to acknowledge the Massachusetts General Hospital pathology core for performing the IHC histology and the Specialized Histopathology Core at Charlestown Navy Yard, Massachusetts General Hospital, for performing the TUNEL staining on the skin graft sections. We would also like to thank the Massachusetts General Hospital flow cytometry core for sorting services.

Address correspondence to: Marcela V. Maus, 149 13th Street, Room 3.216, Charlestown, Massachusetts 02129, USA. Phone: 617.726.5619; Email: mvmaus@mgh.harvard.edu.

1. Sakaguchi S. Regulatory T cells: history and perspective. *Methods Mol Biol*. 2011;707:3–17.
2. Nadig SN, et al. In vivo prevention of transplant arteriosclerosis by ex vivo-expanded human regulatory T cells. *Nat Med*. 2010;16(7):809–813.
3. Mathew JM, et al. A phase I clinical trial with ex vivo expanded recipient regulatory t cells in living donor kidney transplants. *Sci Rep*. 2018;8(1):7428.
4. Taylor PA, Lees CJ, Blazar BR. The infusion of ex vivo activated and expanded CD4(+)CD25(+) immune regulatory cells

inhibits graft-versus-host disease lethality. *Blood*. 2002;99(10):3493–3499.
5. Hoffmann P, Ermann J, Edinger M, Fathman CG, Strober S. Donor-type CD4(+)CD25(+) regulatory T cells suppress lethal acute graft-versus-host disease after allogeneic bone marrow transplantation. *J Exp Med*. 2002;196(3):389–399.
6. Cohen JL, Trenado A, Vasey D, Klatzmann D, Salomon BL. CD4(+)CD25(+) immunoregulatory T Cells: new therapeutics for graft-versus-host disease. *J Exp Med*. 2002;196(3):401–406.
7. Brunstein CG, et al. Umbilical cord blood-derived T regulatory cells to prevent GVHD: kinetics, toxicity profile, and clinical effect. *Blood*. 2016;127(8):1044–1051.
8. Martelli MF, et al. HLA-haploidentical transplantation with regulatory and conventional T-cell adoptive immunotherapy prevents acute leukemia relapse. *Blood*. 2014;124(4):638–644.
9. Kohm AP, Carpentier PA, Anger HA, Miller SD. Cutting edge: $CD4^+CD25^+$ regulatory T cells suppress antigen-specific autoreactive immune responses and central nervous system inflammation during active experimental autoimmune encephalomyelitis. *J Immunol*. 2002;169(9):4712–4716.
10. Bluestone JA, et al. Type 1 diabetes immunotherapy using polyclonal regulatory T cells. *Sci Transl Med*. 2015;7(315):315ra189.
11. Gitelman SE, Bluestone JA. Regulatory T cell therapy for type 1 diabetes: May the force be with you. *J Autoimmun*. 2016;71:78–87.
12. Miyara M, Ito Y, Sakaguchi S. TREG-cell therapies for autoimmune rheumatic diseases. *Nat Rev Rheumatol*. 2014;10(9):543–551.
13. Dominguez-Villar M, Hafler DA. Regulatory T cells in autoimmune disease. *Nat Immunol*. 2018;19(7):665–673.
14. Porter DL, et al. A phase 1 trial of donor lymphocyte infusions expanded and activated ex vivo via CD3/CD28 costimulation. *Blood*. 2006;107(4):1325–1331.
15. Hoeppli RE, MacDonald KG, Levings MK, Cook L. How antigen specificity directs regulatory T-cell function: self, foreign and engineered specificity. *HLA*. 2016;88(1-2):3–13.
16. Dawson NAJ, Vent-Schmidt J, Levings MK. Engineered tolerance: tailoring development, function, and antigen-specificity of regulatory T cells. *Front Immunol*. 2017;8:1460.
17. Wright GP, et al. Adoptive therapy with redirected primary regulatory T cells results in antigen-specific suppression of arthritis. *Proc Natl Acad Sci U S A*. 2009;106(45):19078–19083.
18. Tang Q, Vincenti F. Transplant trials with Tregs: perils and promises. *J Clin Invest*. 2017;127(7):2505–2512.
19. Eshhar Z, et al. The T-body approach: potential for cancer immunotherapy. *Springer Semin Immunopathol*. 1996;18(2):199–209.
20. June CH, O'Connor RS, Kawalekar OU, Ghassemi S, Milone MC. CAR T cell immunotherapy for human cancer. *Science*. 2018;359(6382):1361–1365.
21. Irving BA, Weiss A. The cytoplasmic domain of the T cell receptor zeta chain is sufficient to couple to receptor-associated signal transduction pathways. *Cell*. 1991;64(5):891–901.
22. Eshhar Z, Waks T, Gross G, Schindler DG. Specific activation and targeting of cytotoxic lymphocytes through chimeric single chains consisting of antibody-binding domains and the γ or ζ subunits of the immunoglobulin and T-cell receptors. *Proc Natl Acad Sci U S A*. 1993;90(2):720–724.
23. Milone MC, et al. Chimeric receptors containing CD137 signal transduction domains mediate enhanced survival of T cells and increased antileukemic efficacy in vivo. *Mol Ther*. 2009;17(8):1453–1464.
24. Brentjens RJ, et al. Genetically targeted T cells eradicate systemic acute lymphoblastic leukemia xenografts. *Clin Cancer Res*. 2007;13(18 pt 1):5426–5435.
25. Kalos M, et al. T cells with chimeric antigen receptors have potent antitumor effects and can establish memory in patients with advanced leukemia. *Sci Transl Med*. 2011;3(95):95ra73.
26. Brentjens RJ, et al. CD19-targeted T cells rapidly induce molecular remissions in adults with chemotherapy-refractory acute lymphoblastic leukemia. *Sci Transl Med*. 2013;5(177):177ra38.
27. June CH, Sadelain M. Chimeric antigen receptor therapy. *N Engl J Med*. 2018;379(1):64–73.
28. Kawalekar OU, et al. Distinct signaling of coreceptors regulates specific metabolism pathways and impacts memory development in CAR T cells. *Immunity*. 2016;44(2):380–390.
29. Long AH, et al. 4-1BB costimulation ameliorates T cell exhaustion induced by tonic signaling of chimeric antigen receptors. *Nat Med*. 2015;21(6):581–590.
30. Porter DL, et al. Chimeric antigen receptor T cells persist and induce sustained remissions in relapsed refractory chronic lymphocytic leukemia. *Sci Transl Med*. 2015;7(303):303ra139.
31. MacDonald KG, et al. Alloantigen-specific regulatory T cells generated with a chimeric antigen receptor. *J Clin Invest*. 2016;126(4):1413–1424.
32. Boardman DA, et al. Expression of a chimeric antigen receptor specific for donor HLA class I enhances the potency of human regulatory T cells in preventing human skin transplant rejection. *Am J Transplant*. 2017;17(4):931–943.
33. Yoon J, Schmidt A, Zhang AH, Königs C, Kim YC, Scott DW. FVIII-specific human chimeric antigen receptor T-regulatory cells suppress T- and B-cell responses to FVIII. *Blood*. 2017;129(2):238–245.
34. de Kouchkovsky D, Esensten JH, Rosenthal WL, Morar MM, Bluestone JA, Jeker LT. microRNA-17-92 regulates IL-10 production by regulatory T cells and control of experimental autoimmune encephalomyelitis. *J Immunol*. 2013;191(4):1594–1605.
35. Salomon B, et al. B7/CD28 costimulation is essential for the homeostasis of the $CD4^+CD25^+$ immunoregulatory T cells that control autoimmune diabetes. *Immunity*. 2000;12(4):431–440.
36. Zhang P, et al. Agonistic anti-4-1BB antibody promotes the expansion of natural regulatory T cells while maintaining Foxp3 expression. *Scand J Immunol*. 2007;66(4):435–440.
37. Choi BK, et al. 4-1BB-dependent inhibition of immunosuppression by activated $CD4^+CD25^+$ T cells. *J Leukoc Biol*. 2004;75(5):785–791.
38. Yates K, Bi K, Haining WN, Cantor H, Kim HJ. Comparative transcriptome analysis reveals distinct genetic modules associated with Helios expression in intratumoral regulatory T cells. *Proc Natl Acad Sci U S A*. 2018;115(9):2162–2167.
39. Kmieciak M, et al. Human T cells express CD25 and Foxp3 upon activation and exhibit effector/memory phenotypes without any regulatory/suppressor function. *J Transl Med*. 2009;7:89.
40. Thornton AM, Shevach EM. $CD4^+CD25^+$ immunoregulatory T cells suppress polyclonal T cell activation in vitro by inhibiting interleukin 2 production. *J Exp Med*. 1998;188(2):287–296.

41. Takahashi T, et al. Immunologic self-tolerance maintained by $CD25^+CD4^+$ naturally anergic and suppressive T cells: induction of autoimmune disease by breaking their anergic/suppressive state. *Int Immunol*. 1998;10(12):1969–1980.
42. Nowak A, et al. $CD137^+CD154^-$ expression as a regulatory T cell (Treg)-specific activation signature for identification and sorting of stable human tregs from in vitro expansion cultures. *Front Immunol*. 2018;9:199.
43. Gomes-Silva D, et al. Tonic 4-1BB costimulation in chimeric antigen receptors impedes T cell survival and is vector-dependent. *Cell Rep*. 2017;21(1):17–26.
44. Vignali DA. Mechanisms of T(reg) suppression: still a long way to go. *Front Immunol*. 2012;3:191.
45. Gasteiger G, Kastenmuller W. $Foxp3^+$ regulatory T-cells and IL-2:the Moirai of T-cell fates? *Front Immunol*. 2012;3:179.
46. Thornton AM, Donovan EE, Piccirillo CA, Shevach EM. Cutting edge: IL-2 is critically required for the in vitro activation of $CD4^+CD25^+$ T cell suppressor function. *J Immunol*. 2004;172(11):6519–6523.
47. Sakaguchi S, Wing K, Onishi Y, Prieto-Martin P, Yamaguchi T. Regulatory T cells: how do they suppress immune responses? *Int Immunol*. 2009;21(10):1105–1111.
48. Brodeur ND, Spencer JV. Antibodies to human IL-10 neutralize ebvIL-10-mediated cytokine suppression but have no effect on cmvIL-10 activity. *Virus Res*. 2010;153(2):265–268.
49. Yang Y, et al. TCR engagement negatively affects CD8 but not CD4 CAR T cell expansion and leukemic clearance. *Sci Transl Med*. 2017;9(417):eaag1209.
50. Cao X, et al. Granzyme B and perforin are important for regulatory T cell-mediated suppression of tumor clearance. *Immunity*. 2007;27(4):635–646.
51. Gondek DC, Lu LF, Quezada SA, Sakaguchi S, Noelle RJ. Cutting edge: contact-mediated suppression by $CD4^+CD25^+$ regulatory cells involves a granzyme B-dependent, perforin-independent mechanism. *J Immunol*. 2005;174(4):1783–1786.
52. Vignali DA, Collison LW, Workman CJ. How regulatory T cells work. *Nat Rev Immunol*. 2008;8(7):523–532.
53. Choi BD, et al. Human regulatory T cells kill tumor cells through granzyme-dependent cytotoxicity upon retargeting with a bispecific antibody. *Cancer Immunol Res*. 2013;1(3):163.
54. Sommermeyer D, et al. Fully human CD19-specific chimeric antigen receptors for T-cell therapy. *Leukemia*. 2017;31(10):2191–2199.
55. Johnson LA, et al. Rational development and characterization of humanized anti-EGFR variant III chimeric antigen receptor T cells for glioblastoma. *Sci Transl Med*. 2015;7(275):275ra22.
56. Malek TR, Bayer AL. Tolerance, not immunity, crucially depends on IL-2. *Nat Rev Immunol*. 2004;4(9):665–674.
57. Shevach EM. Application of IL-2 therapy to target T regulatory cell function. *Trends Immunol*. 2012;33(12):626–632.
58. Webster KE, et al. In vivo expansion of T reg cells with IL-2-mAb complexes: induction of resistance to EAE and long-term acceptance of islet allografts without immunosuppression. *J Exp Med*. 2009;206(4):751–760.
59. Hippen KL, et al. Umbilical cord blood regulatory T-cell expansion and functional effects of tumor necrosis factor receptor family members OX40 and 4-1BB expressed on artificial antigen-presenting cells. *Blood*. 2008;112(7):2847–2857.
60. Brentjens RJ, et al. Safety and persistence of adoptively transferred autologous CD19-targeted T cells in patients with relapsed or chemotherapy refractory B-cell leukemias. *Blood*. 2011;118(18):4817–4828.
61. Efimova OV, Kelley TW. Induction of granzyme B expression in T-cell receptor/CD28-stimulated human regulatory T cells is suppressed by inhibitors of the PI3K-mTOR pathway. *BMC Immunol*. 2009;10:59.
62. Scarfo I, et al. Anti-CD37 chimeric antigen receptor T cells are active against B- and T-cell lymphomas. *Blood*. 2018;132(14):1495–1506.